Continuous Time Random Walks for Non-Local Radial Solute Transport

Marco Dentz

Institute of Environmental Assessment and Water Research (IDÆA), Spanish National Research Council (CSIC), 08034 Barcelona, Spain

Peter K. Kang

Massachusetts Institute of Technology, 77 Massachusetts Ave, Building 48, Cambridge, Massachusetts 02139, USA

Tanguy Le Borgne

Université de Rennes 1, CNRS, Geosciences Rennes, UMR 6118, Rennes, France

Abstract

This paper derives and analyzes continuous time random walk (CTRW) models in radial flow geometries for the quantification of non-local solute transport induced by heterogeneous flow distributions and by mobile-immobile mass transfer processes. To this end we derive a general CTRW framework in radial coordinates starting from the random walk equations for radial particle positions and times. The particle density, or solute concentration is governed by a non-local radial advection-dispersion equation (ADE). Unlike in CTRWs for uniform flow scenarios, particle transition times here depend on the radial particle position, which renders the CTRW non-stationary. As a consequence, the memory kernel characterizing the non-local ADE, is radially dependent. Based on this general formulation, we derive radial CTRW implementations that (i) emulate non-local radial transport due to heteroge-

neous advection, (ii) model multirate mass transfer (MRMT) between mobile and immobile continua, and (iii) quantify both heterogeneous advection in a mobile region and mass transfer between mobile and immobile regions. The expected solute breakthrough behavior is studied using numerical random walk particle tracking simulations. This behavior is analyzed by explicit analytical expressions for the asymptotic solute breakthrough curves. We observe clear power-law tails of the solute breakthrough for broad (power-law) distributions of particle transit times (heterogeneous advection) and particle trapping times (MRMT model). The combined model displays two distinct time regimes. An intermediate regime, in which the solute breakthrough is dominated by the particle transit times in the mobile zones, and a late time regime that is governed by the distribution of particle trapping times in immobile zones.

1. Introduction

Solute transport in heterogeneous porous media displays behaviors that cannot be captured by transport models based on an equivalent advection dispersion equation (ADE) parameterized by (constant) effective transport parameters. Such behaviors range from the non-linear evolution of solute dispersion to power-law tails in solute breakthrough curves [1, 2]. The last three decades have seen intense research to quantify these behaviors in terms of effective transport models that can be obtained by moment equation ap-

2

proaches [3], and projector formalisms [4], for example, and include time and space fractional ADEs [5, 6], multirate mass transfer (MRMT) models [7, 8], as well as continuous time random walks [9, 10], see also the reviews in [2, 11, 12].

In this paper, we focus on the CTRW approach to modeling non-Fickian solute transport in heterogeneous media. Classical random walks model particle movements by using variable spatial steps which are taken within constant time increments at equidistant times [13, 14]. A CTRW, in contrast, models particle movements in a heterogeneous medium effectively as a random walk in which both space and time increments are variable. The spatial transitions may reflect the geometry of the underlying medium and flow heterogeneity, while particle transition and waiting times reflect persistent particle velocities over given transition distances, or particle retention due to adsorption or diffusion into immobile zones, for example [9, 15, 16, 17, 18]. The medium heterogeneity is mapped into the probability distribution density (PDF) of characteristic particle transition times. The evolution of the particle density, or, equivalently the solute concentration is governed by a temporally non-local ADE whose memory kernel is given in terms of the PDF of transition times [19, 10].

The MRMT approach is phenomenologically similar to the CTRW modeling framework as it models the impact of medium heterogeneity on large scale transport through a distribution of typical solute retention times in immobile regions. In fact, it can be shown [20, 21] that one model can under certain conditions be mapped onto the other. The latter amounts essentially to identifying the relation between the PDF of particle transition times and

3

particle retention times in immobile regions [22, 23, 24].

As pointed out above, the CTRW model is a random walk approach in that particle movements are governed by random walk equations for the space and time coordinates. Therefore the solution of CTRW and equivalent models is directly accessible to numerical solution through random walk particle tracking simulations [10]. This provides an avenue for the efficient simulation of transport in the presence of mobile-immobile processes [25, 23, 24], for example, and for temporally non-local transport in general [26].

Many formulations of the above models are for transport situations under uniform mean flow. Thus, for the interpretation of tracer tests under forced conditions they are only of limited applicability because the non-stationarity of the underlying flow field is not accounted for. Haggerty et al. [27] use a Eulerian radial MRMT implementation to interpret radial single-well injection-withdrawal (SWIW) tracer tests in fractured dolomite. Le Borgne and Gouze [25] used a CTRW based random walk implementation of MRMT to model tracer breakthrough data from SWIW tracer tests. Benson et al. [6] developed a fractional-order dispersion model in radial coordinates to model tracer tests under forced conditions. A general issue when interpreting field tracer data is to decipher the origin of the observed non-local transport behavior, which may range from mobile-immobile diffusive mass transfer processes to highly heterogeneous advective transport [28, 29]. In the latter case, non-Fickian transport may be caused by a broad distribution of flow and transport velocities; the distribution of particle transit times depends on the flow rate and heterogeneity in the flow properties. In the former case, anomalous transport features are due to mass transfer be-

tween mobiel and immobile zones; particle transition times may depend on the retention properties and geometries of the immobile regions.

Testing these different hypothesis requires non-local transport models, that integrate both diffusive and advective mass transfer processes in non-uniform flow conditions.

In this paper, we develop a general CTRW approach that allows for the modeling of non-local solute transport under radial conditions. The derivation from the space-time random walk equations gives directly the particle tracking method for its numerical solution. We present three non-local CTRW based radial transport implementations, for the modeling of heterogeneous advection, mobile-immobile mass transfer (MRMT), and the combination of both. To this end we review in Section 2 briefly the random walk formulation of general radial advective-dispersive transport. Section 3 then derives the general radial CTRW framework and defines the specific CTRW models. The model breakthrough curves then are analyzed in Section 4 using numerical random walk simulations and explicit analytical expressions for the asymptotic breakthrough behavior developed in Appendix B. In particular, we discuss the expected differences in non-Fickian transport behaviors induced by purely advective processes, purely diffusive processes, and the combination of these processes.

2. Radial Random Walks

The classical advection-dispersion equation (ADE) for the solute concentration $c(r, t)$ in radial coordinates can be written as

$$\frac{\partial c(r, t)}{\partial t} + \frac{1}{r}\frac{\partial}{\partial r}v(r)rc(r, t) - \frac{1}{r}\frac{\partial}{\partial r}rD(r)\frac{\partial c}{\partial r} = 0, \tag{1}$$

where $v(r)$ and $D(r)$ are the radially dependent transport velocity and dispersion coefficient; r denotes the radial distance, t denotes time. We set the constant porosity equal to one, which is equivalent to rescaling time. The equivalent random walk particle tracking formulation is obtained by rewriting (1) in mass conservative form. Therefore, we define the conserved radial concentration as

$$p(r, t) = 2\pi r c(r, t). \qquad (2)$$

Notice that $p(r, t)$ denotes the concentration per unit radial distance. Inserting the latter into (1) and rearranging terms we obtain the radial Fokker-Planck equation

$$\frac{\partial p(r, t)}{\partial t} + \frac{\partial}{\partial r} \left[v(r) + \frac{D(r)}{r} + D'(r) \right] p(r, t) - \frac{\partial^2}{\partial r^2} D(r) p(r, t) = 0, \qquad (3)$$

where $D'(r)$ denotes the derivative of $D(r)$ with respect to r. The equivalent Langevin equation is given by [30]

$$\frac{dr(t)}{dt} = v[r(t)] + \frac{D[r(t)]}{r(t)} + D'[r(t)] + \sqrt{2D[r(t)]}\xi_r(t), \qquad (4)$$

where $\xi_r(t)$ is a Gaussian white noise of zero mean and the correlation function $\langle \xi_r(t)\xi_r(t') \rangle = \delta(t - t')$. Here and in the following, we employ the Ito interpretation [30] of the Langevin equation (4). The particle density is given in terms of the radial trajectories as $p(r, t) = \langle \delta[r - r(t)] \rangle$, and by virtue of (2), we obtain for the concentration distribution

$$c(r, t) = \frac{\langle \delta[r - r(t)] \rangle}{2\pi r}. \qquad (5)$$

In the following, we will consider the case of [31]

$$v(r) = \frac{k_v}{r}, \qquad\qquad D(r) = \frac{\alpha k_v}{r}, \qquad (6)$$

where α is dispersivity, and $k_v = Q/(2\pi)$ with Q the flow rate. Notice that more general radial dependences of flow velocity and dispersion can be considered within the approaches developed in the following. Here, we focus on the choice (6). With these definitions, the Langevin equation (4) simplifies to

$$\frac{dr(t)}{dt} = \frac{k_v}{r(t)} + \sqrt{\frac{2\alpha k_v}{r(t)}}\xi_r(t). \tag{7}$$

The temporally discretized version of the radial Langevin equation is given by

$$r_{n+1} = r_n + \frac{k_v \Delta t}{r_n} + \sqrt{\frac{2\alpha k_v \Delta t}{r_n}}\xi_n, \tag{8}$$

where $r_n = r(t_n)$, $t_n = n\Delta t$, and ξ_n is a Gaussian random variable with zero mean and unit variance.

3. Radial Continuous Time Random Walks

The radial random walk particle tracking formulations developed in the following are based on the generalization of the radial random walk process (8) in terms of the continuous time random walk

$$r_{n+1} = r_n + \ell + \sqrt{2\alpha\ell}\xi_n \tag{9a}$$

$$t_{n+1} = t_n + \tau_n(r), \tag{9b}$$

where ℓ is a constant transition length, and $\tau(r)$ a radially dependent, independently distributed random transition time with the probability density function (PDF) $\psi_\tau(\tau, r)$. Notice that the classical formulation (8) is obtained by setting $\tau_n(r) = \ell r_n/k_v$ in (9). The distribution of the spatial transition

7

lengths $\Delta r = \ell + \sqrt{2\alpha\ell}\xi_n$ is denoted by $\psi_r(\Delta r)$. The mean and mean square displacements are given by $\langle \Delta r \rangle = \ell$ and $\langle \Delta r^2 \rangle = 2\alpha\ell$, where we disregard contributions of order ℓ^2. Notice that the transition length ℓ are chosen such that $\ell \ll \alpha$.

A straightforward application of the general CTRW framework [2] gives for the radial particle density $p(r, t)$ the equation

$$p(r,t) = \int_0^t dt' R(r, t') \int_{t-t'}^\infty d\tau \psi_\tau(\tau, r), \qquad (10)$$

where $R(r, t)$ denotes the probability per time that the particle has just arrived at the radius r. This equation can be read as follows: The particle density at the position r at a time t is given by the probability that a particle arrives there at an earlier time t' times the probability that the next transition takes longer than $t-t'$. The density $R(r, t)$ satisfies the mass balance equation

$$R(r,t) = \delta(r - r_0)\delta(t) + \int_0^\infty dr' \int_0^t dt' R(r', t')\psi_\tau(t - t', r')\psi_r(r - r'), \quad (11)$$

where r_0 is the initial radial particle position. Equations (10) and (11) can be combined into the radial generalized Master equation

$$\frac{dp(r,t)}{dt} = \int_0^\infty dr' \int_0^t dt' \psi_r(r - r')\tau_k(r')^{-1}M(t - t', r')p(r', t')$$

$$- \int_0^t dt' \tau_k(r)^{-1}M(t - t', r)p(r, t), \qquad (12)$$

where the memory kernel $M(t - t', r)$ is defined in Laplace space by

$$\hat{M}(\lambda, r) = \frac{\lambda\tau_k(r)\hat{\psi}_\tau(\lambda, r)}{1 - \hat{\psi}_\tau(\lambda, r)}. \qquad (13)$$

8

The Laplace transform is defined in [32]. Laplace transformed quantities in the following are marked by a hat, the Laplace variable is denoted by λ.

We consider here a $\psi_r(r)$ that is sharply peaked about its mean value ℓ. In this case, the generalized Master equation (12) can be localized in space, and a Taylor expansion of the integrand on the right side of (12) gives the non-local radial Fokker-Planck equation

$$\frac{\partial p(r,t)}{\partial t} + \int_0^t dt' \left(\frac{\partial}{\partial r} \frac{k_v}{r} - \frac{\partial^2}{\partial r^2} \frac{\alpha k_v}{r} \right) M(t-t',r)p(r,t') = 0. \quad (14)$$

We disregard contributions of order ℓ^2. Substituting the radial concentration (2) into this equation, we obtain the non-local radial advection-dispersion equation

$$\frac{\partial c(r,t)}{\partial t} + \int_0^t dt' \left(\frac{k_v}{r} \frac{\partial}{\partial r} - \frac{\alpha k_v}{r} \frac{\partial^2}{\partial r^2} \right) M(t-t',r)c(r,t') = 0. \quad (15)$$

Radial non-local partial differential equations such as (14) and (15) can be solved subject to given initial and boundary conditions, either numerically or semi–analytically using common numerical schemes [6, 33] and analytical methods. In this paper, we use random walk particle tracking to solve for the transport behavior described by these equations.

In the following sections, we present three different models of increasing complexity for the time increment $\tau(r)$. The first one emulates non-local transport due to advective heterogeneity, the second model solves radial transport under multirate mass transfer, the third model provides a random walk approach combining heterogeneous advection and multirate mass transfer into immobile zones in radial coordinates.

3.1. Heterogeneous Advection

We first consider a radial CTRW that represents non-Fickian transport originating from broad distributions of advective transit times. In radial flow conditions, the mean transit time increases linearly with the radial distance. To represent this important property, we propose to scale the random transit time $\tau(r)$ with the characteristic radial transition time $\tau_k(r)$ as

$$\tau(r) = \tau_k(r)\eta, \qquad\qquad \tau_k(r) = \frac{\ell r}{k_v}. \qquad\qquad (16)$$

The time scale $\tau_k(r)$ denotes the transition time over the space increment $\ell \ll r$ under homogeneous flow conditions. The dimensionless random increments η are independent identically distributed according to $\psi_\eta(\eta)$. They reflect the non-dimensional fluctuations of the radial transport velocity due to spatial heterogeneity and are related to the inverse radial flow velocity. Recently, Edery et al. [34] studied the relation of the distribution of hydraulic conductivity and the transition time distribution under uniform flow conditions. The distribution of inverse velocities, and thus transition times, may be obtained from estimates of the hydraulic conductivity distribution. Alternatively it may be modeled by a parametric model [29], whose parameters are adjusted from the observed breakthrough curves, which in turn may give insight into the flow and medium heterogeneity.

Thus, the transition times $\tau(r) = \tau_k(r)\eta$ are distributed according to

$$\psi_\tau(\tau, r) = \frac{1}{\tau_k(r)}\psi_\eta[\tau/\tau_k(r)]. \qquad\qquad (17)$$

The memory kernel $M(t, r)$ defined in the previous section can now be

written as

$$\hat{M}(r,\lambda) = \hat{M}_\eta[\lambda\tau_k(r)] \equiv \frac{\lambda\tau_k(r)\hat{\psi}_\eta[\lambda\tau_k(r)]}{1 - \hat{\psi}_\eta[\lambda\tau_k(r)]}, \qquad (18)$$

where we used that the Laplace transform of (17) is given by $\hat{\psi}(\lambda, r) = \psi_\eta[\lambda\tau_k(r)]$. Thus, it follows that the memory kernel in real time has the scaling form $M(t,r) = \tau_k(r)^{-1}M_\eta[t/\tau_k(r)]$. The generalized advection-dispersion equation (15) can then be written as

$$\frac{\partial c(r,t)}{\partial t} + \int_0^t dt' \left(\frac{k_v}{r}\frac{\partial}{\partial r} - \frac{\alpha k_v}{r}\frac{\partial^2}{\partial r^2}\right)\frac{M_\eta[(t-t')/\tau_k(r)]}{\tau_k(r)}c(r,t') = 0. \qquad (19)$$

Notice the exponential distribution $\psi_\eta(\eta) = \exp(-\eta)$ gives $M_\eta(\eta) = \delta(\eta)$ in (18) and thus the generalized radial advection-dispersion equation (19) reduces to the radial advection-dispersion equation (1) in a homogeneous medium.

3.2. Multirate Mass Transfer

The MRMT model considers solute transport under mass transfer between a single mobile zone and a series of immobile zones [7, 35, 8, 21, 20, 33]. Here we derive a radial random walk approach that simulates mass transfer between mobile and immobile regions based on the radial CTRW (9) and the CTRW model presented in the previous section. An important difference with the advective CTRW model described in the previous section is that the distribution of trapping times does not depend on the radial position.

Mass transfer between mobile and immobile regions is modeled by a compound Poisson process for the transition time $\tau(r)$ following the works of [22], [23] and [24]. The particle transition time $\tau(r)$ is split into a mobile time

11

$\tau_m(r)$, which is the time the particle needs to traverse the distance ℓ in the mobile portion of the medium, and a series of immobile times $\tau_{im,i}$, which measure the times the particles spent in the immobile portion of the medium. The number of times n_{im} a particle gets trapped during a mobile transition of duration $\tau_m(r)$ is given by a Poisson distribution characterized by the mean $\gamma\tau_m(r)$, where γ is the rate by which particles get trapped in immobile zones,

$$P_{im}[n, \tau_m(r)] = \frac{[\gamma\tau_m(r)]^n}{n!} \exp\left[-\gamma\tau_m(r)\right]. \tag{20}$$

Thus, the time increment $\tau(r)$ in (9b) associated to the spatial transition (9a) is given by

$$\tau(r) = \tau_m(r) + \sum_{i=1}^{n_{im}} \tau_{im,i}. \tag{21}$$

The distribution of immobile times is denoted by $p_{im}(\tau)$. For simplicity, we consider here the situation that initially all particles are mobile. The mobile times are given by $\tau_m(r) = \tau_k(r)\eta$ as in (16), with an exponentially distributed η. Notice that, as pointed out at the end of the previous section, an exponential η models transport in a homogeneous medium. This means, $\tau_m(r)$ is exponentially distributed with mean $\tau_k(r)$. Thus the transition time PDF can be expressed in terms of its Laplace transform as (see Appendix A)

$$\hat{\psi}_\tau(\lambda, r) = \frac{1}{1 + \lambda\tau_k(r) + \gamma\tau_k(r)[1 - \hat{p}_{im}(\lambda)]}. \tag{22}$$

Inserting this expression into (13) for the Laplace transform $\hat{M}(\lambda, r)$ of the memory kernel gives the compact expression

$$\hat{M}(\lambda, r) \equiv \hat{M}(\lambda) = \frac{1}{1 + \gamma\lambda^{-1}[1 - \hat{p}_{im}(\lambda)]}. \tag{23}$$

12

Note that the memory kernel is independent on the radial distance, which reflects the difference between mobile particle transitions, which depends on the local flow velocity, and particle retention in immobile zones, which depends on the distribution of diffusion times, for example. Using this expression in the Laplace transform of (15) gives for the radial concentration

$$\lambda \hat{c}(r, \lambda) + \left(\frac{k_v}{r} \frac{\partial}{\partial r} - \frac{\alpha k_v}{r} \frac{\partial^2}{\partial r^2} \right) \frac{\hat{c}(r, \lambda)}{1 + \gamma \lambda^{-1}[1 - \hat{p}_{im}(\lambda)]} = c(r, t = 0). \quad (24)$$

We define now the mobile solute concentration by its Laplace transforms as

$$\hat{c}_m(r, \lambda) = \frac{\hat{c}(r, \lambda)}{1 + \gamma \lambda^{-1}[1 - \hat{p}_{im}(\lambda)]}. \quad (25)$$

Thus, we obtain from (24) for $\hat{c}_m(r, \lambda)$

$$\lambda \hat{c}_m(r, \lambda) + \lambda \left\{ \gamma \lambda^{-1}[1 - \hat{p}_{im}(\lambda)]\hat{c}_m(r, \lambda) \right\}$$
$$+ \left(\frac{k_v}{r} \frac{\partial}{\partial r} - \frac{\alpha k_v}{r} \frac{\partial^2}{\partial r^2} \right) \hat{c}(r, \lambda) = c_m(r, t = 0). \quad (26)$$

Note that we assume for simplicity that initially all particles are mobile. An initial presence of particles in the immobile zones would give rise to a source term in (26) [36]. We furthermore define the density of immobile particles by the expression in curly brackets on the left side of (26). It reads in time space as

$$c_{im}(r, t) = \gamma \int_0^t dt' c_m(r, t') \int_{t-t'}^{\infty} d\tau p_{im}(\tau). \quad (27)$$

The right hand side expresses the density of immobile particles by the probability per time that mobile particles get trapped at a given time t', $\gamma c_m(r, t')$, times the probability that the residence time in the immobile region is larger

13

than $t - t'$. Thus, at asymptotically long times, the ratio of the time averaged immobile and mobile concentrations is given by

$$\lim_{t \to \infty} \frac{\overline{c}_{im}(r, t)}{\overline{c}_m(r, t)} = \lim_{\lambda \to 0} \gamma \lambda^{-1} [1 - p_{im}^*(\lambda)] = \gamma \langle \tau_{im} \rangle, \qquad (28)$$

where $\langle \tau_{im} \rangle$ is the mean immobile time and the overline denotes the time average $\overline{c}(r, t) = t^{-1} \int_0^t dt' c(r, t')$.

We now define the memory function $\varphi(t)$ as

$$\varphi(t) = \frac{1}{\langle \tau_{im} \rangle} \int_t^\infty d\tau \, p_{im}(\tau). \qquad (29)$$

Thus, the governing equation (26) of the mobile solute concentration can be written in time space as

$$\frac{\partial c_m(r, t)}{\partial t} + \beta \int_0^t dt' \varphi(t - t') c_m(r, t') + \left(\frac{k_v}{r} \frac{\partial}{\partial r} - \frac{\alpha k_v}{r} \frac{\partial^2}{\partial r^2} \right) c(r, t) = 0. \quad (30)$$

where we defined $\beta = \gamma \langle \tau_{im} \rangle$. Equation (30) describes transport under multirate mass transfer in radial flow [27, 25]. The memory function $\varphi(t)$ encodes the mass transfer mechanism [7, 35, 8, 21, 37] between the mobile and immobile regions. For linear first-order mass exchange it reflects the distribution of transfer rates between mobile and immobile regions [7]. For diffusive mass transfer, it encodes the geometries and the characteristic diffusion scales of the immobile regions [38, 39]. For transport through highly heterogeneous porous and fractured media, the memory function may be related semi-analytically or empirically to the medium heterogeneity [40, 41].

The memory function is here defined in terms of the distribution of residence times in the immobile regions given by (29). Reversely, the distribution

14

of residence times $p_{im}(\tau)$ can be obtained for a given memory function $\varphi(t)$ according to

$$p_{im}(\tau) = -\langle \tau_{im} \rangle \frac{d\varphi(\tau)}{d\tau}. \tag{31}$$

Expressions (29) and (31) establish the relation between the distribution of residence times and the memory function.

3.3. Combination of Heterogeneous Advection and Multirate Mass Transfer

We consider now the random walk implementation of the combination of CTRW, which accounts for heterogeneous transport in the mobile zone, and multirate mass transfer between the mobile and immobile regions. Using the approach presented in the previous section, the mobile transition time $\tau_m(r)$ in (21) is now given by the general relationship $\tau_m(r) = \tau_k(r)\eta$. The random variable η is distributed according to a general $\psi_\eta(\eta)$ as outlined in Section 3.1. Accordingly, the PDF for the mobile transitions is given by (17) and reads as

$$\psi_m(\tau, r) = \frac{1}{\tau_k(r)} \psi_\eta[\tau/\tau_k(r)]. \tag{32}$$

Thus, the transition time PDF for the general compound (21) process reads in terms of its Laplace transform as (see Appendix A)

$$\hat{\psi}_\tau(\lambda, r) = \hat{\psi}_m\left(\lambda + \gamma[1 - \hat{p}_{im}(\lambda)], r\right). \tag{33}$$

Specifically, by using the Laplace transform of (32), $\hat{\psi}_m(\lambda, t) = \hat{\psi}_\eta[\lambda \tau_k(t)]$, the Laplace transform of $\psi_\tau(\tau, r)$ can be written as

$$\hat{\psi}_\tau(\lambda, r) = \hat{\psi}_\eta\left(\lambda \tau_k(r) + \gamma \tau_k(r)[1 - \hat{p}_{im}(\lambda)], r\right). \tag{34}$$

15

Note that unlike for the mobile immobile model discussed in the previous section, the transition time PDF renders the memory kernel (13) dependent on the radial distance. The total trapping time during a mobile transition is related to the number of trapping events, whose mean is given by the mobile transition time times the trapping rate. While the individual trapping times are independent on advective heterogeneity, their collective is related to advective heterogeneity through the number of trapping event. This interrelation is reflected in the radial dependence of (34).

For times $t \ll \gamma^{-1}$, or equivalently $\lambda \gg \gamma$, the transition time PDF (34) can be approximated by the one for purely advective heterogeneity. Thus for $t \ll \gamma^{-1}$, transport is dominated by advective heterogeneity, which is evident because at $t \ll \gamma^{-1}$ the number of trapping events is very small. If the PDF of dimensionless mobile transition times $\psi_\eta(\eta)$ has the finite mean transition time $\langle \eta \rangle < \infty$, the transition time PDF (34) can be approximated for small arguments as

$$\hat{\psi}_\tau(\lambda, r) = 1 - \tau_k(r)\langle \eta \rangle \lambda \left\{ 1 + \lambda^{-1}\gamma[1 - \hat{p}_{im}(\lambda)] \right\}. \tag{35}$$

Notice that this is valid as long as $\lambda \tau_k(r) + \gamma \tau_k(r)[1 - \hat{p}_{im}(\lambda)] \ll 1$. Inserting (35) into (13) gives in leading order for the memory kernel

$$\hat{M}(\lambda, r) \equiv \hat{M}(\lambda) = \langle \eta \rangle^{-1} \frac{1}{1 + \gamma\lambda^{-1}[1 - \hat{p}_{im}(\lambda)]}. \tag{36}$$

Thus, in this limit, the model behaves as the MRMT model introduced in the previous section. These asymptotic behaviors of the different models are discussed in more detail in the next section, which studies solute breakthrough in the presented CTRW models.

4. Breakthrough Curves

We discuss here the behavior of solute breakthrough curves in the radial non-local models developed in the previous section for an instantaneous pulse tracer injection at radius $r = r_0$. Notice that the response to a pulse has a fundamental character because responses to other injection conditions can be obtained by superposition of pulse responses. Furthermore, in field tracer experiments the duration of the tracer pulse is typically much shorter than the duration of the experiment and may be approximated as instantaneous [28, 6, 29].

We use numerical random walk particle tracking simulations to solve for the breakthrough behavior in each of the models and derive explicit analytical expressions for their asymptotic behaviors. The numerical simulations are based on the recursion relations (9) for the particle positions and times. Specifically, the initial position at $n = 0$ random walk steps is set to $r_0 = \ell$ and the initial time is set to $t_0 = 0$.

The solute breakthrough curve is identical to the distribution $f(t, r)$ of first passage times of solute particles at the radius r. The first passage time $\tau_a(r)$ is defined by

$$\tau_a(r) = t_{n_r} \tag{37}$$

where $n_r = \min(n | r_n \geq r)$ denotes the minimum number of steps needed to pass the radius r. The first passage time PDF then is given by

$$f(t, r) = \sum_{n=0}^{\infty} f_0(n, r) p(t, n), \tag{38}$$

17

where $f_0(n,r)$ denotes the distribution of the minimum number of steps needed to exceed r, and $p(t,n)$ the distribution of times after n random walk steps in (9b).

4.1. Heterogeneous Advection

The CTRW approach representing heterogeneous advection models the transition time by the time increment (16), which is determined by the dimensionless increment η. In the following, we consider for $\psi_\eta(\eta)$ the Pareto distribution

$$\psi_\eta(\eta) = \beta\eta^{-1-\beta}, \qquad\qquad \eta \geq 1, \qquad\qquad (39)$$

which models a broad distribution of transport velocities. This type of pure power-law behavior may be observed in an intermediate time regime. Asymptotically one would expect that the transition time PDF is truncated on a scale corresponding to a largest heterogeneity scale, for example, see also the discussion in [10].

For a power-law distribution $\psi_\eta(\eta)$ of dimensionless transition times, we derive in Appendix B.1 the following scaling forms of the breakthrough curves for times larger than $\tau_k(r)$

$$f(t,r) = \frac{1}{\theta(r)} f_{01}\left[\frac{t}{\theta(r)}\right], \qquad\qquad 0 < \beta < 1 \qquad\qquad (40)$$

$$f(t,r) = \frac{1}{\theta(r)} f_{02}\left[\frac{t - \langle\tau_a(r)\rangle}{\theta(r)}\right], \qquad\qquad 1 < \beta < 2, \qquad\qquad (41)$$

where we defined

$$\theta(r) = \left[\sum_{i=1}^{r/\ell} \tau_k(r_i)^\beta\right]^{1/\beta}, \qquad\qquad \langle\tau_a(r)\rangle = \frac{1}{\beta-1}\sum_{i=1}^{r/\ell} \tau_k(r_i). \qquad (42)$$

18

We furthermore obtain for the asymptotic behavior of the scaling functions $f_{01}(x)$ and $f_{02}(x)$ for $x \gg 1$ the power-law decay $\sim x^{-1-\beta}$ such that we obtain for $t \gg \theta(r)$ the following behavior for the breakthrough curves

$$f(t,r) \sim \frac{1}{\theta(r)} \left[\frac{t}{\theta(r)} \right]^{-1-\beta}. \tag{43}$$

For $0 < \beta < 1$, mean and variance of the arrival time do not exist, for $1 < \beta < 2$, the mean exists and is given by $\langle \tau_a(r) \rangle$, while the variance diverges. The mean arrival time depends on distribution of transition times through $\beta - 1$ in the denominator. The second term in the expression for $\langle \tau_a(r) \rangle$ is the mean arrival time for a homogeneous model characterized by an exponential PDF of dimensionless transition times η. For $0 < \beta < 1$, the characteristic time $\theta(r)$ scales peak width and position, as can be deduced from the scaling form (40). For $1 < \beta < 2$, it is a measure for the peak width, as indicated by (41). Using $\tau_k(r) = \ell r / k_v$, we obtain for $\theta(r)$ and $\langle \tau_a(r) \rangle$

$$\theta(r) \approx \frac{\ell^2}{k_v} \left(\frac{1}{1+\beta} \right)^{1/\beta} \left(\frac{r}{\ell} \right)^{1+1/\beta}, \qquad \langle \tau_a(r) \rangle \approx \frac{1}{\beta - 1} \frac{r^2}{2k_v}. \tag{44}$$

Note that the late time scaling (43) is the same as for a uniform flow scenario that is characterized by a power-law distribution of transition times [10]. The radial geometry is reflected in the dependence of the characteristic time scales (42) on r.

Figure 1 shows solute breakthrough curves for different values of dispersivity α and exponents β of the Pareto distribution (39). The width of the peak of the breakthrough curves increases with increasing α, as shown in Figure 1a. The peak arrival time remains unaffected by α. Figure 1 shows the behavior of the breakthrough curves for different exponents β. With
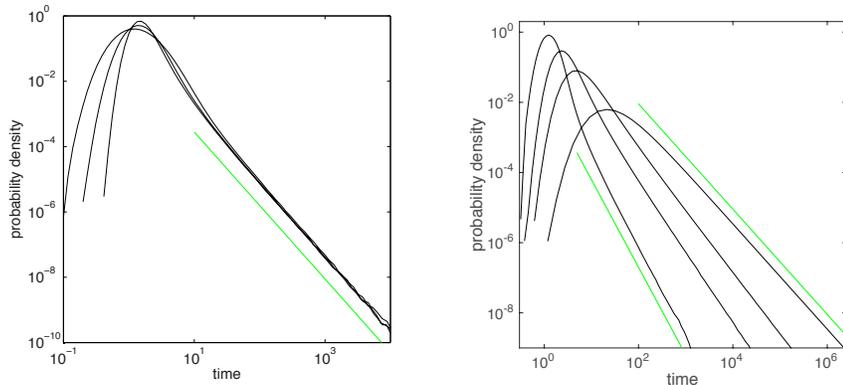
19

Figure 1: Breakthrough curves for the CTRW model (16) with (a) $\alpha = 10^{-2}, 4\times10^{-2}, 10^{-1}$, $\beta = 5/4$, and (b) (from left to right) $\beta = 3/2, 1, 3/4, 1/2$, and $\alpha = 2 \times 10^{-2}$. The peak width in (a) increases with increasing α. The green lines show the power-law $\sim t^{-1-\beta}$ behaviors for (a) $\beta = 5/4$ and (b) $\beta = 1/2$ and $\beta = 3/2$.

increasing β, the peak arrival time and the width of the breakthrough peak both decrease as indicated by (44). For times $t \gg \tau_k(r)$ we clearly observe the power-law behavior (43). As outlined above, the late time power-law behavior is the same as the one observed for uniform form. The scaling of peak arrival and width, however, are impacted on by both the radial geometry and the transition time PDF, as given in (42).

4.2. Multirate Mass Transfer

The CTRW model for multirate mobile-immobile mass exchange is characterized by the transition times (21). The mobile times are given by $\tau_m(r) = \tau_k(r)\eta$, where η here is distributed according to the exponential PDF

$$\psi_\eta(\eta) = \exp(-\eta). \tag{45}$$

The distribution of immobile times $p_{im}(\tau)$ is given by the Pareto distribution

$$p_{im}(\tau) = \frac{\delta}{\tau_c} \left(\frac{\tau}{\tau_c}\right)^{-1-\delta}, \qquad\qquad \tau \geq \tau_c. \qquad (46)$$

Notice that the memory function $\varphi(t)$ for diffusive mass transfer between a mobile and homogeneous immobile zones behaves as $\varphi(t) \sim t^{-1/2}$ [7, 8]. Thus, we obtain from (31) that the corresponding PDF of immobile times behaves as $p_{im}(\tau) \sim t^{-3/2}$, which corresponds to $\delta = 1/2$ in (46). For heterogeneous immobile zones, one obtains in general different behaviors for the memory function $\varphi(t)$ [39] and therefore for the PDF of immobile times. The asymptotic behavior of the breakthrough curves for times $t \gg \tau_c$ is derived in Appendix B.2. It is given by

$$f(t, r) \sim \frac{1}{\theta_c(r)} \left[\frac{t}{\theta_c(r)}\right]^{-1-\delta}, \qquad \theta_c(r) = \tau_c \left[\gamma \sum_{i=1}^{r/\ell} \tau_k(i\ell)\right]^{1/\delta}. \qquad (47)$$

Recall that γ is the rate for trapping in the immobile zones. The characteristic time $\theta_c(r)$ is a measure for peak width and the time for the onset of the power-law tail behavior $f(t, r) \sim t^{-1-\delta}$. Using the explicit $\tau_k(r) = \ell r/k_v$ gives for $\theta_c(r)$

$$\theta_c(r) \approx \tau_c \left(\frac{\gamma r^2}{2k_v}\right)^{1/\delta} \qquad (48)$$

Figure 2 shows the behavior of the breakthrough curves for $\delta = 1/2$ and varying dispersivity α and trapping rate γ. As for the case of heterogeneous advection, increase in dispersivity α leads to an increase of the width of the breakthrough peak, as illustrated in Figure 2a. The peak arrival time remains unchanged. Figure 2b shows solute breakthrough curves for varying trapping rates γ. As γ increases, the weight in the power-law tail increases as well
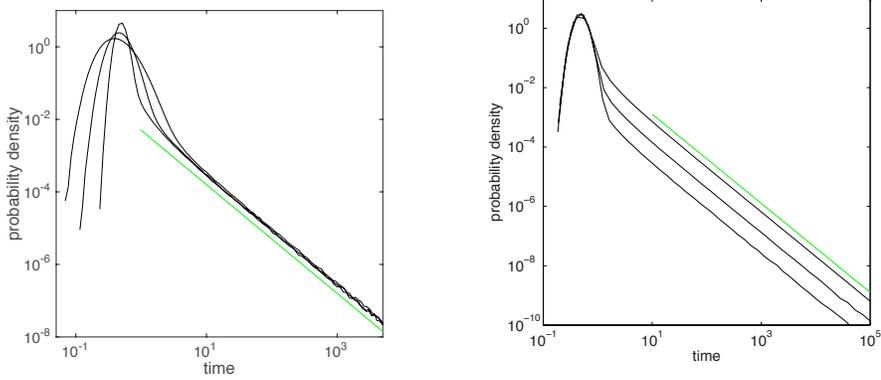
21

Figure 2: Breakthrough curves for the MRMT model (21) with (a) $\alpha = 10^{-2}, 4 \times 10^{-2}, 10^{-1}$, $\delta = 1/2$, $\tau_c = 10^{-1}$ and $\gamma = 10^{-1}$, and (b) $\alpha = 2 \times 10^{-2}$, $\delta = 1/2$, $\tau_c = 10^{-1}$ and $\gamma = 10^{-2}, 5 \times 10^{-2}, 2.5 \times 10^{-1}$. The green lines show the power-law $\sim t^{-1-\delta}$ behavior for $\delta = 1/2$.

as the peak width and therefore also the time of the onset of the power-law behavior. Note that increasing the trapping rate increases the proportion of trapped particles at any time, which explains the increased weight in the tail of the breakthrough curve. At the same time, increasing γ decreases the time that particles spend mobile, and thus particularly the average time until which particles get trapped for the first time. Thus, as particles notice the presence of immobile zones earlier, the peak width increases, and the breakthrough curve breaks off earlier from the behavior without immobile zones.

4.3. Heterogeneous Advection with Multirate Mass Transfer

The CTRW model combining heterogeneous advection in the mobile zone with mass exchange between mobile and immobile regions is based on the transition times (21). The mobile time increment is again given by $\tau_m(r) =$

$\tau_k(r)\eta$, where η now is modeled by the Pareto distribution (39) character-
ized by the exponent β. The PDF of immobile times is again given by the
Pareto distribution (46) characterized by the exponent δ. We focus here
on situations, for which $\beta > \delta$. Notice that the exponents β and δ encode
the width of the distributions of characteristic advection scales and trapping
time scales, respectively. The width of characteristic trapping time scales is
typically larger than the one of characteristic advection time scales in the
mobile zone, and thus we set $\beta > \delta$.

Appendix B.3 develops the asymptotic breakthrough behavior for this
model. One can distinguish two time regimes with distinct temporal behav-
ior. An intermediate time regime is set by the advection scale $\tau_k(r)$ and
the immobile time scale $\hat{\tau}_{im} = \tau_c(\alpha_{im}\gamma\tau_c)^{\frac{1}{\delta-1}}$ for $\tau_k(r) \ll \hat{\tau}_{im}$. We con-
sider the case $0 < \delta < 1$ such that this condition can only be achieved for
$\gamma\tau_c \ll 1$, which implies a low trapping rate. Thus, in this time regime,
most particles have not yet encountered a trapping event and thus, the
breakthrough curve behaves as in the case of heterogeneous advection given
by (43), $f(t,r) \sim t^{-1-\beta}$.

In the long time regime $t \gg \hat{\tau}_{im}$, we need to distinguish between the
cases $0 < \beta < 1$ and $1 < \beta < 2$. For $0 < \beta < 1$, the long time breakthrough
behavior is given by

$$f(t,r) \sim t^{-1-\beta\delta}. \tag{49}$$

Note that $0 < \beta < 1$ indicates quite strong tailing in the mobile zone.
Thus both the exponents characteristic for the mobile and immobile zones
determine the long time breakthrough behavior. For $1 < \beta < 2$ the long time
breakthrough behavior is dominated by particle retention due to trapping in
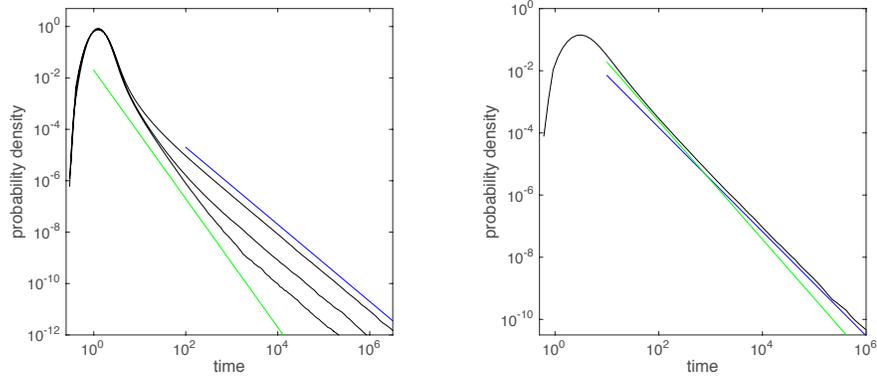
Figure 3: Breakthrough curves for the combined model (21) with (a) $\alpha = 2 \times 10^{-2}$, $\beta = 3/2$, $\delta = 1/2$, $\tau_c = 1$ and (from top to bottom) $\gamma = 10^{-2}, 10^{-3}, 10^{-4}$, (b) $\alpha = 2 \times 10^{-2}$, $\beta = 0.9$, $\delta = 3/4$, $\tau_c = 1$ and $\gamma = 5 \times 10^{-2}$. The green lines indicates the power-law $\sim t^{-1-\beta}$ for (a) $\beta = 3/2$ and (b) $\beta = 0.9$. The blue line in (a) indicates the power-law $\sim t^{-1-\delta}$ for $\delta = 1/2$. The blue line in (b) indicates the power-law $\sim t^{-1-\beta\delta}$ for $\beta = 0.9$ and $\delta = 3/4$.

the immobile regions. The breakthrough curve behaves asymptotically as given by (47).

These behaviors are illustrated in Figure 3. Figure 3a shows the behaviors in the intermediate and asymptotic long-time regimes for $\beta = 3/2$ and $\delta = 1/2$. We see a relatively short intermediate regime (which increases as the trapping rate γ decreases) dominated by the advective heterogeneity and a the long time regime dominated by particle retention in the immobile regions. A very similar behavior has been observed in the field from push pull tracer tests [25] pointing to a combined effect of advective and diffusive processes on non-Fickian transport. Figure 3b illustrates the breakthrough curve for $\beta = 0.9$ and $\delta = 0.75$. The intermediate time regime again is dominated by the advective heterogeneity while the asymptotic tailing behavior is determined

by both the advective and trapping exponents.

5. Summary and Conclusions

The CTRW approach provides a versatile framework for the modeling of non-Fickian solute transport in heterogeneous media. In this paper we develop a general CTRW approach for transport under radial flow conditions starting from the random walk equations for the radial and temporal particle coordinates. In contrast to CTRW formulations under uniform flow conditions here the random transition times form a non-stationary stochastic process, which reflects the radial dependence, i.e., non-stationarity, of the flow conditions. Thus, the evolution of the solute concentration is governed by a non-local ADE that is characterized by a radially dependent memory kernel. Within this general framework, we present CTRW models that may account for the impact of advective heterogeneity on large scale transport, that implement multirate mass transfer between a mobile immobile regions, and that combine non-local mobile transport due to heterogeneous advection and mass transfer into immobile zones. The three models are characterized by the specific forms of the stochastic process of particle times.

For heterogeneous advection, the transition time reflects the inverse (heterogeneous) flow velocity, which in average depends on the total flow rate and on the radial distance. This is accounted for by a transition time that is modeled as the product of a non-dimensional time increment and an advective transition time that is proportional to the radial distance and the inverse flow rate. Thus, transition times decrease with increasing flow rate as expected for purely advective heterogeneity. Flow heterogeneity is accounted

for by the distribution of the dimensionless time increment [29]. The memory kernel of the non-local ADE for solute concentration depends here on the radial distance.

Radial transport under multirate mass transfer between mobile and immobile regions is implemented by separating the transition time into the time the particle is mobile and the sum of immobile times, which is represented by a compound Poisson process [22, 23] whose mean is given by the trapping rate times the local mobile trapping time. The mobile time is modeled by an exponentially distributed dimensionless time increment, which models Fickian mobile transport. The mean number of trapping events during a mobile transition is given by the trapping rate and the mean mobile time. The memory kernel here is independent of the radial distance, which reflects the fact that the individual trapping events do not depend on mobile advection, which is consistent with radial MRMT formulation that assume homogeneous advection in the mobile zone [27].

Finally, we propose a CTRW model that combines heterogeneous advection in the mobile continuum with multirate mass transfer into immobile continua. The mobile transition time now is modeled by a non-exponential dimensionless time increment. The immobile time increment is again a compound Poisson process. While the individual trapping events are independent on the heterogeneous advection, the collective of trapping times depends on the radial distance through the mean number of trapping events. Unlike for the case of a homogeneous mobile advection, heterogeneity leads to an interrelation of the PDFs of mobile transition times and retention times in immobile regions, and thus to a radial dependence of the memory kernel.

The derivation of the general framework from the random walk equations for the particle coordinates in space and time provides directly the random walk particle tracking methods for the numerical solution of radial MRMT models, and temporally non-local radial transport formulations in general. Notice that the developed non-local transport models assume that dispersion is proportional to the flow velocity, as well as a constant injection or withdrawal rate of the flow at the well. It is straightforward to relax the first assumption and introduce a more general velocity dependence of dispersion in the developed models. The assumption of a constant flow rate may be relaxed to account for scenarios encountered in single well injection withdrawal tests, i.e., piecewise constant flow rates.

The solute breakthrough behaviors for the different non-local radial transport models are studied in detail by using random walk particle tracking simulations and explicit analytical expressions for the asymptotic time behaviors of the solute breakthrough curves. A broad distribution of advective transition times is modeled by a Pareto distributions of dimensionless times. The distribution of immobile times is also given by a Pareto distribution, which mimics a broad distribution of diffusion or in general retention times in the immobile zones. We find distinct power-law tail behavior in all cases, which are similar to the ones that can be observed for uniform flow. However, the non-stationarity of the random time increment leads to a non-trivial radial dependence of the breakthrough curves. The model combining heterogeneous advection and MRMT can display an intermediate time regime in which heterogeneous advection dominates, before the onset of trapping, and a late time regime that is governed by the retention properties in the im-

27

mobile regions. The different behaviors in the two time-regimes allow for the discrimination and identification of heterogeneous advection and mobile-immobile mass transfer as drivers of anomalous transport. The CTRW model accounting for advective heterogeneity is controlled by the flow rate, while the CTRW model for MRMT is controlled by the trapping rate and the properties of the immobile zone.

In conclusion, this paper provides a radial CTRW framework that allows for the systematic interpretation of tracer data from radial forced gradient test, through the implementation of different mechanisms that lead to non-local radial transport.

Appendix A. Derivation of the Transition Time Distribution for the Compound Time Process

We derive here the probability density function (PDF) $\psi(t, r)$ for the general compound process (21) of the time increment $\tau(r)$. The density of the mobile time $\tau_m(r) = \tau_k(r)\eta$ is denoted by $\psi_m(\tau, r)$, and can be expressed in terms of the PDF $\psi_\eta(\eta)$ as

$$\psi_m(\tau, r) = \frac{1}{\tau_k(r)} \psi_\eta[\tau/\tau_k(r)]. \tag{A.1}$$

The density of the compound process $\tau(r)$ can be written in general as

$$\psi_\tau(\tau, r) = \langle \delta[\tau - \tau(r)] \rangle, \tag{A.2}$$

28

where the angular brackets denote the ensemble average over all particles. Inserting (21) and performing the average over the $\tau_m(r)$ gives

$$\psi_\tau(\tau, r) = \int_0^\infty d\tau_m \psi_m(\tau_m, r) \left\langle \delta \left(\tau - \tau_m - \sum_{i=1}^{n_{im}} \tau_{im,i} \right) \right\rangle \qquad (A.3)$$

Performing the Laplace transform in τ and performing the average of the $\tau_{im,i}$ gives

$$\hat{\psi}_\tau(\lambda, r) = \int_0^\infty d\tau_m \psi_m(\tau_m) \exp(-\lambda \tau_m) \langle \hat{p}_{im}(\lambda)^{n_{im}} \rangle. \qquad (A.4)$$

Performing the average of the Poisson variable n_{im} results in

$$\hat{\psi}_\tau(\lambda, r) = \int_0^\infty d\tau_m \psi_m(\tau_m) \sum_{n=0}^\infty \frac{\hat{p}_{im}(\lambda)^n (\gamma \tau_m)^n}{n!} \exp[-(\lambda + \gamma)\tau_m]. \qquad (A.5)$$

The infinite series can be summed up to an exponential such that

$$\hat{\psi}_\tau(\lambda, r) = \int_0^\infty d\tau_m \psi_m(\tau_m) \exp\left(- \{\lambda + \gamma[1 - \hat{p}_{im}(\lambda)]\} \tau_m \right). \qquad (A.6)$$

The integration over τ_m can be performed explicitly by noting that the integral is equal to the Laplace transform of $\psi_m(\tau_m, r)$. Thus we obtain directly (33). Using the Laplace transform of the exponential distribution $\psi_m(\tau_m, r) = \tau_k(r)^{-1} \exp[-\tau_m/\tau_k(r)]$,

$$\hat{\psi}_m(\lambda, r) = \frac{1}{1 + \lambda \tau_k(r)} \qquad (A.7)$$

gives directly (22).

Appendix B. Asymptotic Behavior

We consider now the asymptotic long time behavior of the breakthrough curves for the CTRW models presented in Sections 3.1, 3.2 and 3.3. The distribution $f(t, r)$ of arrival times at a radius r is given by

$$f(t, r) = \sum_{n=0}^{\infty} f_0(n, r) p(t, n), \tag{B.1}$$

where $f_0(n, r)$ is the distribution of the number of steps needed to arrive at the radius r in the random walk (9a), and $p(t, n)$ the distribution of times needed to make n steps in the random walk (9b). For large n it can be approximated by an inverse Gaussian distribution that is sharply peaked about $n = r/\ell$. Thus, we approximate the breakthrough curve by

$$f(t, r) \approx p(t, r/\ell). \tag{B.2}$$

In the following, we derive the asymptotic behavior of $p(t, n)$ for large times t. Notice that $p(t, n)$ can be defined by

$$p(t, n) = \langle \delta(t - t_n) \rangle, \tag{B.3}$$

where t_n is given by (9b) and can be written as

$$t_n = \sum_{i=0}^{n-1} \tau_i(r_i). \tag{B.4}$$

Thus, the Laplace transform of $p(t, n)$ can be written as

$$\hat{p}(\lambda, n) = \left\langle \exp\left[-\lambda \sum_{i=0}^{n-1} \tau_i(r_i) \right] \right\rangle = \prod_{i=0}^{n-1} \hat{\psi}(\lambda, r_i), \tag{B.5}$$

30

where $\hat{\psi}(\lambda, r_i)$ is given by

$$\hat{\psi}(\lambda, r_i) = \langle \exp\left[-\lambda \tau_i(r_i)\right]\rangle. \tag{B.6}$$

Equation (B.5) can also be written as

$$\hat{p}(\lambda, n) = \exp\left\{\sum_{i=0}^{n-1} \ln[\hat{\psi}(\lambda, r_i)]\right\}, \tag{B.7}$$

We note that $\hat{\psi}(\lambda, r_i) = 1 + \Delta\hat{\psi}(\lambda, r_i)$, where $\Delta\hat{\psi}(\lambda, r_i)$ decreases with decreasing λ, see below. Thus, for small λ, we can approximate

$$\hat{p}(\lambda, n) = \exp\left[\sum_{i=0}^{n-1} \Delta\psi(\lambda, r_i)\right], \tag{B.8}$$

The asymptotic behavior will be determined starting from expression (B.6) for the density of a single radial transition time.

Appendix B.1. Heterogeneous Advection Model

For the CTRW model defined through (16), the single transition time $\tau_i(r_i)$ is defined by

$$\tau_i(r_i) = \tau_k(r_i)\eta_i. \tag{B.9}$$

The random variable η_i is distributed according to a power-law such that

$$\psi_\eta(\eta) \sim \eta^{-1-\beta}, \tag{B.10}$$

for large η and $0 < \beta < 2$. Thus, (B.6) can be written as

$$\hat{\psi}(\lambda, r_i) = \langle \exp\left[-\lambda \tau_k(r_i)\eta_i\right]\rangle = \hat{\psi}_\eta[\lambda \tau_k(r_i)]. \tag{B.11}$$

Notice that the Laplace transform of the power-law density (B.10) can be expanded for small λ as [e.g., 10]

$$\hat{\psi}_\eta(\lambda) = 1 - \alpha_{11}\lambda^\beta, \qquad\qquad 0 < \beta < 1 \qquad\qquad \text{(B.12)}$$

$$\hat{\psi}_\eta(\lambda) = 1 - \alpha_{12}\lambda + \alpha_{22}\lambda^\beta, \qquad\qquad 1 < \beta < 2, \qquad\qquad \text{(B.13)}$$

where the parameters α_{11}, α_{12} and α_{22} depend on the details of the underlying distribution $\psi_\eta(\eta)$. For the Pareto distribution (39), they are given by

$$\alpha_{11} = \Gamma(1 - \beta), \qquad\qquad\qquad\qquad\qquad \text{(B.14)}$$

$$\alpha_{12} = \frac{1}{\beta - 1}, \qquad\qquad \alpha_{22} = \frac{\Gamma(2 - \beta)}{\beta - 1}. \qquad\qquad \text{(B.15)}$$

Thus, $\hat{\psi}(\lambda, r_i)$ can be approximated for $\lambda\tau_k(r_i) \ll 1$ as

$$\hat{\psi}(\lambda, r_i) = 1 - \alpha_{11}[\lambda\tau_k(r_i)]^\beta, \qquad\qquad 0 < \beta < 1 \qquad\qquad \text{(B.16a)}$$

$$\hat{\psi}(\lambda, r_i) = 1 - \alpha_{12}\lambda\tau_k(r_i) + \alpha_{22}[\lambda\tau_k(r_i)]^\beta, \qquad 1 < \beta < 2. \qquad\qquad \text{(B.16b)}$$

Inserting the latter into (B.8) gives

$$\hat{p}(\lambda, n) = \exp\left[-\alpha_{11}(\lambda\theta_n)^\beta\right], \qquad\qquad 0 < \beta < 1 \qquad\qquad \text{(B.17)}$$

$$\hat{p}(\lambda, n) = \exp\left[-\lambda\langle\tau_{a,n}\rangle + \alpha_{22}(\lambda\theta_n)^\beta\right], \qquad 1 < \beta < 2, \qquad\qquad \text{(B.18)}$$

where we defined

$$\theta_n = \left[\sum_{i=1}^n \tau_k(r_i)^\beta\right]^{1/\beta}, \qquad\qquad \langle\tau_{a,n}\rangle = \alpha_{12}\sum_{i=1}^n \tau_k(r_i). \qquad\qquad \text{(B.19)}$$

The latter is the mean arrival time, which is only defined for $1 < \beta < 2$. It is impacted on by the distribution of dimensionless transition times through α_{12}. For $\alpha_{12} = 1$, it is equal to the mean arrival time of the homogeneous

32

model. From (B.17) and (B.18), we can deduce the scaling forms

$$p(t,n) = \frac{1}{\theta_n} f_{01}(t/\theta_n), \qquad\qquad 0 < \beta < 1 \qquad\qquad (\text{B.20})$$

$$p(t,n) = \frac{1}{\theta_n} f_{02}\left(\frac{t - \langle \tau_{a,n} \rangle}{\theta_n}\right), \qquad 1 < \beta < 2, \qquad\qquad (\text{B.21})$$

where the Laplace transforms of $f_{01}(t)$ and $f_{02}(t)$ are defined by

$$\hat{f}_{01}(\lambda) = \exp\left(-\alpha_{11}\lambda^\beta\right), \qquad\qquad 0 < \beta < 1 \qquad\qquad (\text{B.22})$$

$$\hat{f}_{02}(\lambda) = \exp\left(\alpha_{22}\lambda^\beta\right), \qquad\qquad 1 < \beta < 2, \qquad\qquad (\text{B.23})$$

We obtain the long-time behavior of the breakthrough curves by expanding the latter expressions up to leading order in $\lambda \ll 1$, which gives

$$\hat{f}_{01}(\lambda) = 1 - \alpha_{11}\lambda^\beta, \qquad\qquad 0 < \beta < 1 \qquad\qquad (\text{B.24})$$

$$\hat{f}_{02}(\lambda) = 1 + \alpha_{22}\lambda^\beta, \qquad\qquad 1 < \beta < 2. \qquad\qquad (\text{B.25})$$

Thus, $f_{01}(t)$ and $f_{02}(t)$ behave at long times as $\sim t^{-1-\beta}$ and thus $p(t,n)$ behaves for $t \gg \theta_n$ as

$$p(t,n) \sim \frac{1}{\theta_n}\left(\frac{t}{\theta_n}\right)^{-1-\beta}, \qquad\qquad (\text{B.26})$$

Expression (43) is obtained by setting $n = r/\ell$, $r_i = i\ell$, and $\theta(r) = \theta_{r/\ell}$.

Appendix B.2. MRMT Model

We employ for the trapping time distribution $p_{im}(\tau)$ the power-law

$$p_{im}(\tau) \sim \frac{1}{\tau_c}\left(\frac{t}{\tau_c}\right)^{-1-\delta}, \qquad\qquad (\text{B.27})$$

for $t \gg \tau_c$, τ_c a characteristic immobile time and $0 < \delta < 1$. Thus, its Laplace transform for $\lambda\tau_c \ll 1$ can be written as

$$\hat{p}_{im}(\lambda) = 1 - \alpha_{im}(\lambda\tau_c)^\delta. \qquad\qquad (\text{B.28})$$

Inserting the latter into (22) for the transition time distribution and expanding the resulting expression up to the leading order, we obtain

$$\hat{\psi}_\tau(\lambda, r_i) = 1 - \gamma \tau_k(r_i) \alpha_{im}(\lambda \tau_c)^\delta. \tag{B.29}$$

Using this expression in (B.5) and again expanding to leading order yields for $\hat{p}(\lambda, n)$

$$\hat{p}(\lambda, n) = 1 - \alpha_{im}(\lambda \tau_c)^\delta \gamma \sum_{i=1}^n \tau_k(r_i), \tag{B.30}$$

where α_{im} is given by the details of $p_{im}(\tau)$. Thus, the asymptotic behavior of $p(t, n)$ is given by

$$p(t, n) \sim \frac{1}{\theta_{c,n}} \left(\frac{t}{\theta_{c,n}} \right)^{-1-\delta}, \qquad \theta_{c,n} = \tau_c \left[\gamma \sum_{i=1}^n \tau_k(r_i) \right]^{1/\delta}. \tag{B.31}$$

Expression (47) is obtained by setting $r_i = i\ell$, $n = r/\ell$ and $\theta_c(r) = \theta_{c,r/\ell}$.

Appendix B.3. Heterogeneous Advection with MRMT

We consider now the case that the mobile transition time is given by (B.9) with η distributed according to the power-law (B.10). For the immobile times with use the distribution (B.27). Thus, the Laplace transforms of the distributions of the mobile transition time and the immobile times are given by (B.16) and (B.28), respectively. Using (B.28) in (33) gives for the transition time distribution

$$\hat{\psi}_\tau(\lambda, r) = \hat{\psi}_m \left(\lambda + \gamma \alpha_{im}(\lambda \tau_c)^\delta, r \right). \tag{B.32}$$

Using now expansion (B.16) for $\hat{\psi}_\tau(\lambda, r)$ gives

$$\hat{\psi}_\tau(\lambda, r_i) = 1 - \alpha_1 \left\{ \left[\lambda + \gamma \alpha_{im} (\lambda \tau_c)^\delta \right] \tau_k(r_i) \right\}^\beta, \qquad 0 < \beta < 1 \qquad \text{(B.33a)}$$

$$\hat{\psi}_\tau(\lambda, r_i) = 1 - \alpha_1 \left[\lambda + \gamma \alpha_{im} (\lambda \tau_c)^\delta \right] \tau_k(r_i)$$
$$+ \alpha_2 \left\{ \left[\lambda + \gamma \alpha_{im} (\lambda \tau_c)^\delta \right] \tau_k(r_i) \right\}^\beta, \qquad 1 < \beta < 2. \qquad \text{(B.33b)}$$

From these expressions, we can identify two characteristic times scales that separate time regimes with different behaviors. The first one is set by the condition

$$\lambda \gg (\alpha_{im} \gamma \tau_c)^{\frac{1}{1-\delta}} \tau_c^{-1}, \qquad \text{(B.34)}$$

which implies that

$$t \ll \tau_c \left(\alpha_{im} \gamma \tau_c \right)^{\frac{1}{\delta-1}}. \qquad \text{(B.35)}$$

The second time scale is set by the condition that $\lambda \tau_k(r_i) \ll 1$, which implies

$$t \gg \tau_k(r_i). \qquad \text{(B.36)}$$

These scales set the time regimes $\tau_k(r_i) \ll t \ll \tau_c \left(\alpha_{im} \gamma \tau_c \right)^{\frac{1}{\delta-1}}$, and $t \gg \tau_c \left(\alpha_{im} \gamma \tau_c \right)^{\frac{1}{\delta-1}}$.

In the regime $(\alpha_{im} \gamma \tau_c)^{\frac{1}{1-\delta}} \tau_c^{-1} \ll \lambda \ll \tau_k(r)^{-1}$, the transition time density $\hat{\psi}(\lambda, r_i)$ is given in leading order by

$$\hat{\psi}_\tau(\lambda, r_i) = 1 - \alpha_1 \left[\lambda \tau_k(r_i) \right]^\beta, \qquad\qquad 0 < \beta < 1 \qquad \text{(B.37a)}$$

$$\hat{\psi}_\tau(\lambda, r_i) = 1 - \alpha_1 \lambda \tau_k(r_i) + \alpha_2 \left[\lambda \tau_k(r_i) \right]^\beta, \qquad 1 < \beta < 2, \qquad \text{(B.37b)}$$

which is identical to (B.16). Thus, the breakthrough curves for $\tau_k(r) \ll t \ll \tau_c \left(\alpha_{im} \gamma \tau_c \right)^{\frac{1}{\delta-1}}$ behave as in (B.26).

35

In the long time regime $t \gg \tau_c (\alpha_{im} \gamma \tau_c)^{\frac{1}{\delta-1}}$, we need to distinguish between the cases $0 < \beta < 1$ and $1 < \beta < 2$. In the former case, the leading order of $\hat{\psi}_\tau(\lambda, r_i)$ for $\lambda \ll (\alpha_{im} \gamma \tau_c)^{\frac{1}{1-\delta}} \tau_c^{-1}$ is given by

$$\hat{\psi}_\tau(\lambda, r_i) = 1 - \alpha_1 \alpha_{im}^\beta [\gamma \tau_k(r_i)]^\beta (\lambda \tau_c)^{\beta \delta}. \tag{B.38}$$

Inserting this expression into (B.5) and expanding up to leading order gives for $\hat{p}(\lambda, n)$

$$\hat{p}(\lambda, n) = 1 - \alpha_1 \alpha_{im}^\beta (\lambda \tau_c)^{\beta \delta} \sum_{i=1}^{n} [\gamma \tau_k(r_i)]^\beta. \tag{B.39}$$

Thus, $p(t, n)$ behaves asymptotically as

$$p(t, n) \sim t^{-1-\beta \delta}. \tag{B.40}$$

In the case $1 < \beta < 2$, the leading order of $\hat{\psi}(\lambda, r_i)$ for $\lambda \ll (\alpha_{im} \gamma \tau_c)^{\frac{1}{1-\delta}} \tau_c^{-1}$ is given by

$$\hat{\psi}(\lambda, r_i) = 1 - \alpha_1 \alpha_{im} (\lambda \tau_c)^\delta \gamma \tau_k(r_i). \tag{B.41}$$

Inserting this expression into (B.5) and expanding up to leading order gives for $\hat{p}(\lambda, n)$ similar as in the previous section

$$\hat{p}(\lambda, n) = 1 - \alpha_1 \alpha_{im} (\lambda \tau_c)^\delta \gamma \sum_{i=1}^{n} \tau_k(r_i). \tag{B.42}$$

Thus, the asymptotic behavior of $p(t, n)$ is given by (B.31).

[1] J. P. Bouchaud, A. Georges, Anomalous diffusion in disordered media: Statistical mechanisms, models and physical applications, Phys. Rep. 195 (4,5) (1990) 127–293. doi:10.1016/0370-1573(90)90099-N.

[2] B. Berkowitz, A. Cortis, M. Dentz, H. Scher, Modeling non-Fickian transport in geological formations as a continuous time random walk, Rev. Geophys. 44 (2) (2006) RG2003. doi:10.1029/2005RG000178.

[3] S. P. Neuman, C. L. Winter, C. M. Newman, Stochastic-theory of field scale Fickian dispersion in anisotropic porous media, Water Resour. Res. 23 (1987) 453466. doi:10.1029/WR023i003p00453.

[4] J. Cushman, X. Hu, T. Ginn, Nonequilibrium statistical mechanics of preasymptotic dispersion, J. Stat. Phys. 75 (5-6) (1994) 859–878. doi:10.1007/BF02186747.
URL http://dx.doi.org/10.1007/BF02186747

[5] D. A. Benson, S. W. Wheatcraft, M. M. Meerschaert, Application of a fractional advection-dispersion equation, Water Resour. Res. 36 (6) (2000) 1403–1412. doi:10.1029/2000WR900031.
URL http://dx.doi.org/10.1029/2000WR900031

[6] D. A. Benson, C. Tadjeran, M. M. Meerschaert, I. Farnham, G. Pohll, Radial fractional-order dispersion through fractured rock, Water Resour. Res. 40 (12) (2004) W12416, w12416. doi:10.1029/2004WR003314.
URL http://dx.doi.org/10.1029/2004WR003314

[7] R. Haggerty, S. M. Gorelick, Multiple-rate mass transfer for modeling diffusion and surface reactions in media with pore-scale heterogeneity, Water Resour. Res. 31 (10) (1995) 2383–2400. doi:10.1029/95WR10583.
URL http://dx.doi.org/10.1029/95WR10583

[8] J. Carrera, X. Sánchez-Vila, I. Benet, A. Medina, G. Galarza, J. Guimerà, On matrix diffusion: formulations, solution methods and qualitative effects, Hydrogeol. J. 6 (1) (1998) 178–190. doi:10.1007/s100400050143.
URL http://dx.doi.org/10.1007/s100400050143

[9] B. Berkowitz, H. Scher, Anomalous transport in random fracture networks, Phys. Rev. Lett. 79 (1997) 4038–4041. doi:10.1103/PhysRevLett.79.4038.
URL http://link.aps.org/doi/10.1103/PhysRevLett.79.4038

[10] M. Dentz, A. Cortis, H. Scher, B. Berkowitz, Time behavior of solute transport in heterogeneous media: transition from anomalous to normal transport, Adv. Water Resour. 27 (2) (2004) 155 – 173. doi:10.1016/j.advwatres.2003.11.002.
URL http://www.sciencedirect.com/science/article/pii/S0309170803001726

[11] S. P. Neuman, D. M. Tartakovsky, Perspective on theories of anomalous transport in heterogeneous media, Adv. Water Resour. 32 (2008) 670–680. doi:10.1016/j.advwatres.2008.08.005.

[12] M. Dentz, T. LeBorgne, A. Englert, B. Bijeljic, Mixing, spreading and reaction in heterogeneous media: A brief review, J. Cont. Hydrol. 120-121 (2011) 1–17. doi:10.1016/j.jconhyd.2010.05.002.

[13] F. Delay, P. Ackerer, C. Danquigny, Simulating solute transport in porous or fractured formations using random walk parti-

cle tracking: A review, Vadose Zone Journal 4 (2005) 360–379. doi:10.2136/vzj2004.0125.

[14] P. Salamon, D. Fernàndez-Garcia, G.-H. J. J., A review and numerical assessment of the random walk particle tracking methods, J. Cont. Hydrol. 87 (2006) 277–305. doi:10.1016/j.jconhyd.2006.05.005.

[15] T. Le Borgne, M. Dentz, J. Carrera, Lagrangian statistical model for transport in highly heterogeneous velocity fields, Phys. Rev. Lett. 101 (2008) 090601. doi:10.1103/PhysRevLett.101.090601.

[16] M. Dentz, A. Castro, Effective transport dynamics in porous media with heterogeneous retardation properties, Geophys. Res. Lett. 36 (2009) L03403. doi:10.1029/2008GL036846.

[17] M. Dentz, D. Bolster, Distribution- versus correlation-induced anomalous transport in quenched random velocity fields, Phys. Rev. Lett. 105 (2010) 244301. doi:10.1103/PhysRevLett.105.244301.

[18] P. K. Kang, M. Dentz, T. Le Borgne, R. Juanes, Spatial Markov model of anomalous transport through random lattice networks, Phys. Rev. Lett. 107 (2011) 180602. doi:10.1103/PhysRevLett.107.180602.

[19] B. Berkowitz, J. Klafter, R. Metzler, H. Scher, Physical pictures of transport in heterogeneous media: Advection-dispersion, random-walk, and fractional derivative formulations, Water Resour. Res. 38 (10) (2002) 1191. doi:10.1029/2001WR001030.

[20] R. Schumer, D. A. Benson, M. M. Meerschaert, B. Baeumer, Fractal

mobile/immobile solute transport, Water Resour. Res. 39 (2003) 10. doi:10.1029/2003WR002141.

[21] M. Dentz, B. Berkowitz, Transport behavior of a passive solute in continuous time random walks and multirate mass transfer, Water Resour. Res. 39 (2003) 1111. doi:10.1029/2001WR001163.

[22] G. Margolin, M. Dentz, B. Berkowitz, Continuous time random walk and multirate mass transfer modeling of sorption, Chem. Phys. 295 (2003) 71–80. doi:10.1016/j.chemphys.2003.08.007.

[23] D. A. Benson, M. M. Meerschaert, A simple and efficient random walk solution of multi-rate mobile/immobile mass transport equations, Adv. Water Resour. 32 (2009) 532539. doi:10.1016/j.advwatres.2009.01.002.

[24] M. Dentz, P. Gouze, A. Russian, J. Dweik, F. Delay, Diffusion and trapping in heterogeneous media: An inhomogeneous continuous time random walk approach, Adv. Water Resour. 49 (2012) 13–22. doi:10.1016/j.advwatres.2012.07.015.

[25] T. Le Borgne, P. Gouze, Non-Fickian dispersion in porous media: 2. model validation from measurements at different scales., Water Resour. Res. 44 (2007) W06427. doi:10.1029/2007WR006279.

[26] Y. Zhang, D. A. Benson, Lagrangian simulation of multidimensional anomalous transport at the made site, Geophys. Res. Lett. 35 (2008) L07403. doi:10.1029/2008GL033222.

[27] R. Haggerty, S. W. Fleming, L. C. Meigs, S. A. McKenna, Tracer tests in a fractured dolomite 2. analysis of mass transfer in single-well

injection-withdrawal tests, Water Resour. Res. 37 (2001) 1129–1142. doi:10.1029/2000WR900334.

[28] M. W. Becker, A. M. Shapiro, Interpreting tracer breakthrough tailing from different forced- gradient tracer experiment configurations in fractured bedrock, Water Resour. Res. 39 (2003) 1024. doi:10.1029/2001WR001190.

[29] P. K. Kang, T. Le Borgne, M. Dentz, O. Bour, R. Juanes, Impact of velocity correlation and distribution on transport in fractured media: field evidence and theoretical model, Water Resour. Res. 51 (2015) 940–959. doi:10.1002/ 2014WR015799.

[30] H. Risken, The Fokker-Planck Equation, Springer Heidelberg New York, 1996.

[31] J. Bear, Dynamics of fluids in porous media, American Elsevier, New York, 1972.

[32] M. Abramowitz, I. A. Stegun, Handbook of Mathematical Functions, Dover Publications, New York, 1972.

[33] O. Silva, J. Carrera, D. M., S. Kumar, A. Alcolea, M. Willmann, A general real-time formulation for multi-rate mass transfer problems, Hydrol. Earth Syst. Sci. 13 (2009) 1399–1411. doi:10.5194/hess-13-1399-2009.

[34] Y. Edery, A. Guadagnini, H. Scher, B. Berkowitz, Origins of anomalous transport in heterogeneous media: Structural and dynamic controls, Water Resour. Res. 50. doi:10.1002/2013WR015111.

[35] C. F. Harvey, S. M. Gorelick, Temporal moment-generating equations: Modeling transport and mass transfer in heterogeneous aquifers, Water Resour. Res. 31 (8) (1995) 1895–1911. doi:10.1029/95WR01231.

[36] J. Tecklenburg, I. Neuweiler, M. Dentz, J. Carrera, S. Geiger, C. Abramowski, O. Silva, A non-local two-phase flow model for immiscible displacement in highly heterogeneous porous media and its parametrization, Adv. Water Resour. 62 (2013) 475487. doi:10.1016/j.advwatres.2013.05.012.

[37] M. Dentz, P. Gouze, J. Carrera, Effective non-local reaction kinetics for transport in physically and chemically heterogeneous media, J. Cont. Hydrol. 120-121 (2011) 222236. doi:10.1016/j.jconhyd.2010.06.002.

[38] B. Noetinger, T. Estebenet, Up-scaling of double porosity fractured media using continuous-time random walks methods, Transp. Porous Media 39 (2000) 315–337. doi:10.1023/A:1006639025910.

[39] P. Gouze, Z. Melean, T. Le Borgne, M. Dentz, J. Carrera, Non-fickian dispersion in porous media explained by heterogeneous microscale matrix diffusion, Water Resour. Res. 44 (2008) W11416. doi:10.1029/2007WR006690.

[40] M. Willmann, J. Carrera, X. Sanchez-Vila, Transport upscaling in heterogeneous aquifers: What physical parameters control memory functions?, Water Resour. Res. 44 (2008) W12437. doi:10.1029/2007WR006531.

[41] Y. Zhang, C. T. Green, B. Baeumer, Linking aquifer spatial properties and non-Fickian transport in mobile–immobile like alluvial settings, J. Hydrol. 512 (2014) 315–331. doi:10.1016/j.jhydrol.2014.02.064.